



## RESEARCH ARTICLE

10.1002/2017GC006892

## Key Points:

- We present the first volcanic gas compositional time-series taken prior to a paroxysmal eruption of Villarrica volcano (Chile)
- We find evidence for a gas CO<sub>2</sub>/SO<sub>2</sub> ratio precursor to eruption of a carbon-poor arc magma
- We interpret preeruptive evolution toward CO<sub>2</sub>-enriched gas as caused by supply of deeply sourced gas bubbles

## Correspondence to:

A. Aiuppa,  
alessandro.aiuppa@unipa.it

## Citation:









Aiuppa, A., et al. (2017), A CO<sub>2</sub>-gas precursor to the March 2015 Villarrica volcano eruption, *Geochem. Geophys. Geosyst.*, 18, doi:10.1002/2017GC006892.

Received 27 FEB 2017

Accepted 10 MAY 2017

Accepted article online 22 MAY 2017

A CO<sub>2</sub>-gas precursor to the March 2015 Villarrica volcano eruption

Alessandro Aiuppa<sup>1,2</sup> , Marcello Bitetto<sup>1</sup> , Vincenzo Francofonte<sup>2</sup>, Gabriela Velasquez<sup>3</sup>, Claudia Bucarey Parra<sup>3</sup>, Gaetano Giudice<sup>2</sup> , Marco Liuzzo<sup>2</sup> , Roberto Moretti<sup>4</sup> , Yves Moussallam<sup>5</sup>, Nial Peters<sup>5</sup> , Giancarlo Tamburello<sup>1,6</sup> , Oscar. A. Valderrama<sup>3</sup> , and Aaron Curtis<sup>7</sup>
<sup>1</sup>Dipartimento DiSTeM, Università di Palermo, Palermo, Italy, <sup>2</sup>Istituto Nazionale di Geofisica e Vulcanologia, Sezione di Palermo, Palermo, Italy, <sup>3</sup>Observatorio Vulcanológico de los Andes del Sur (OVDAS), Servicio Nacional de Geología y Minería, Temuco, Chile, <sup>4</sup>Dipartimento di Ingegneria Civile Design, Edilizia e Ambiente Seconda Università degli Studi di Napoli, Naples, Italy, <sup>5</sup>Department of Geography, University of Cambridge, Downing Place, Cambridge, UK, <sup>6</sup>Istituto Nazionale di Geofisica e Vulcanologia, Sezione di Bologna, Bologna, Italy, <sup>7</sup>Department of Earth and Environmental Science, New Mexico Institute of Mining and Technology, Socorro, New Mexico, USA

**Abstract** We present here the first volcanic gas compositional time-series taken prior to a paroxysmal eruption of Villarrica volcano (Chile). Our gas plume observations were obtained using a fully autonomous Multi-component Gas Analyser System (Multi-GAS) in the 3 month-long phase of escalating volcanic activity that culminated into the 3 March 2015 paroxysm, the largest since 1985. Our results demonstrate a temporal evolution of volcanic plume composition, from low CO<sub>2</sub>/SO<sub>2</sub> ratios (0.65–2.7) during November 2014–January 2015 to CO<sub>2</sub>/SO<sub>2</sub> ratios up to ≈ 9 then after. The H<sub>2</sub>O/CO<sub>2</sub> ratio simultaneously declined to <38 in the same temporal interval. We use results of volatile saturation models to demonstrate that this evolution toward CO<sub>2</sub>-enriched gas was likely caused by unusual supply of deeply sourced gas bubbles. We propose that separate ascent of over-pressured gas bubbles, originating from at least 20–35 MPa pressures, was the driver for activity escalation toward the 3 March climax.

## 1. Introduction

Recent advances in instrumental monitoring of volcanic gas compositions have markedly improved our ability to track preeruptive degassing of magmas, and therefore to interpret and predict transition from quiescence to volcanic eruption [Edmonds, 2008; Oppenheimer et al., 2014; Aiuppa, 2015; Fischer and Chiodini, 2015]. The advent of the Multi-component Gas Analyzer System (Multi-GAS) [Aiuppa et al., 2005; Shinohara, 2005] in the past decade has enabled systematic measurement of volcanic CO<sub>2</sub>/SO<sub>2</sub> gas ratios at high temporal resolution, and represents a major breakthrough for volcanic gas studies. The temporally resolved volcanic gas time-series contributed by permanent Multi-GAS networks have allowed capturing the passive degassing of CO<sub>2</sub>-rich gas prior to eruption of mafic arc volcanoes [e.g., Aiuppa et al., 2007]. High temporal resolution gas measurements initially focused on Italian volcanoes, where the first permanent MultiGAS networks were installed [Aiuppa et al., 2009, 2010a, 2010b], and where a peculiar CO<sub>2</sub>-rich magmatism [Métrich et al., 2004; Kamenetsky et al., 2007] makes gas CO<sub>2</sub>/SO<sub>2</sub> ratios a particularly suitable monitoring parameter. Recent work at Redoubt in the Aleutians [Werner et al., 2013], Bezymianny in Kamchatka [Lopez et al., 2013], and Turrialba in Costa Rica [de Moor et al., 2016], all belonging to the category of CO<sub>2</sub>-poor (Group 1) volcanoes of Aiuppa et al., [2015, 2017], indicates that precursory changes in the volcanic gas CO<sub>2</sub>/SO<sub>2</sub> ratio do occur in wide-ranging volcano contexts.

The Southern Volcanic Zone (SVZ) of the southern Andes [Hildreth and Moor bath, 1988; Stern, 2004] is an arc segment where volcanic gases have been found especially poor in carbon [Shinohara and Witter, 2005; Tamburello et al., 2014, 2015], possibly due to marginal limestones in the subducted sedimentary succession [Plank, 2014]. Geochemical studies on erupted magmas [Jacques et al., 2013; Wehrmann et al., 2014] are also consistent with a relatively modest addition of sediment-derived slab fluids to SVZ magmas, at least relative to other arc segments (e.g., the Central American Volcanic Arc [Sadofsky et al., 2008]). Villarrica volcano in Chile (39.42°S, 71.93°W; Figure 1) is the strongest volcanic gas source within the SVZ, and is

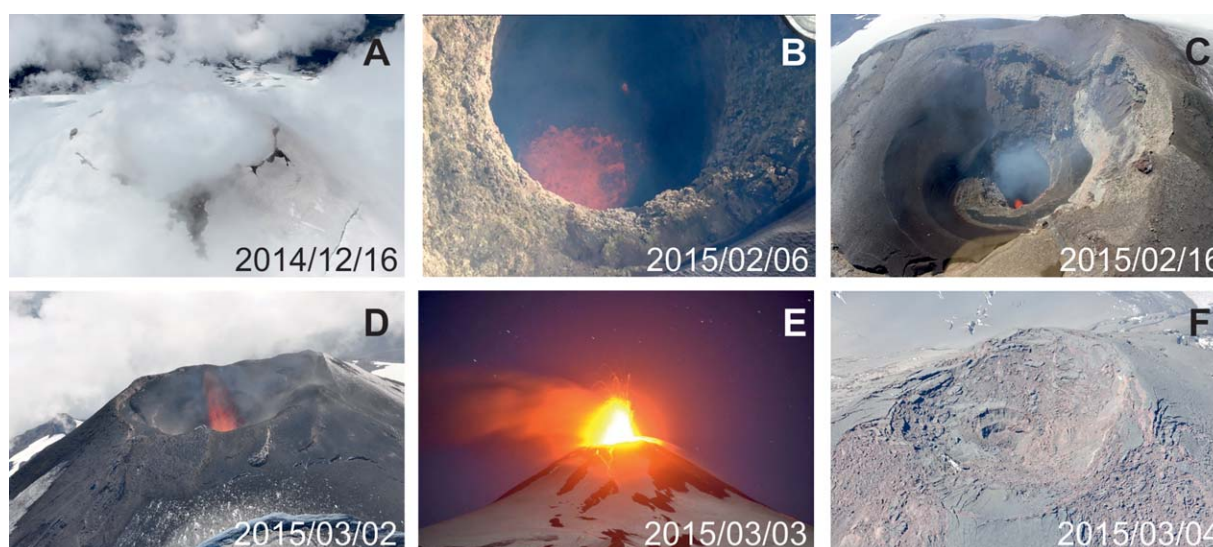


**Figure 1.** Image sequence showing evolution of Villarrica volcano throughout December 2014 to March 2015. Dates are in the yyyy/mm/dd format. (a) Quiescent degassing activity in mid-December 2014; (b) and (c) more vigorous lava lake activity (seething magma) in early to mid-February 2015; (d) intense strombolian activity on 2 March 2015; (e) the paroxysmal lava fountaining activity in the night of 3 March; (f) the post-paroxysm summit of Villarrica on 4 March.

world-renowned for its persistent open-vent lava-lake activity [Moreno *et al.*, 1994; Witter *et al.*, 2004; Palma *et al.*, 2008]. Owing to its glaciated nature and relatively difficult accessibility, Villarrica has been targeted by sporadic volcanic gas surveys, but not systematically monitored with permanent instrumentation [Witter *et al.*, 2004; Mather *et al.*, 2004; Shinohara and Witter, 2005; Palma *et al.*, 2008; Sawyer *et al.*, 2011; Moussallam *et al.*, 2016]. Unfortunately, no volcanic gas report exists that characterizes degassing activity prior to the paroxysmal explosions that occasionally interrupt the normal, mild lava lake activity.

Here, we present new Multi-GAS-based observations of the Villarrica volcanic gas plume, taken in the months/days before the volcano's latest paroxysm in early March 2015 [Global Volcanism Program (GVP), 2016]. Our observations, covering a period of  $\sim 3$  months, improve the currently sparse volcanic gas data set for this unique but remote volcano. On a broader scale, our results contribute to a better understanding of lava-lake degassing dynamics [Sawyer *et al.*, 2008a, 2008b; Oppenheimer *et al.*, 2009, 2011; Martin *et al.*, 2010; Moussallam *et al.*, 2014, 2015, 2016; Allard *et al.*, 2015, 2016; Molina *et al.*, 2015].

## 2. Villarrica Volcano

Villarrica is a 2847 m high, partially glaciated strato-volcano [Moreno *et al.*, 1994], famous for hosting one of the few examples of open-vent lava lakes on Earth [Francis *et al.*, 1993]. The Villarrica lava lake is typically 20–30m wide, and is located at depths of 50 to  $>150$ m within a funnel-shaped summit crater (Figure 1). The lake underlies a overhung spatter roof, grown from repeated accumulation and agglutination of ejected spatter [Palma *et al.*, 2008; Goto and Johnson, 2011]. The regular Villarrica activity is dominated by continuous quiescent outgassing, sustained by convective over-turning of the shallow lava lake reservoir [Witter *et al.*, 2004; Ripepe *et al.*, 2010]. A variety of bubble bursting activities are also observed at the lake surface, including small strombolian bursts and 10–20m high lava fountains [Calder *et al.*, 2004; Palma *et al.*, 2008]. Intensity of such bubble bursting activity fluctuates over time, and vigorous phases are typically associated with higher levels of seismic tremor,  $\text{SO}_2$  flux and seismo-acoustic activity [Palma *et al.*, 2008; Richardson *et al.*, 2014].

This regular activity is occasionally interrupted, at intervals of every few decades on average [Van Daele *et al.*, 2014], by paroxysmal eruptive periods, punctuated by  $\text{VEI} \approx 2$  explosive events and lahars. Lake core sediment records indicate that at least 22 such paroxysmal lahar-forming eruptions have occurred during the last 600 years [Van Daele *et al.*, 2014], most recently in 1971, 1984–1985, and March 2015 [Johnson and Palma, 2015]. The 3 March 2015 paroxysmal eruption interrupted a period of  $> 20$  years of regular activity following the 1984–1985 and 1991 eruptions [GVP, 2013]. The paroxysmal phase was preceded by

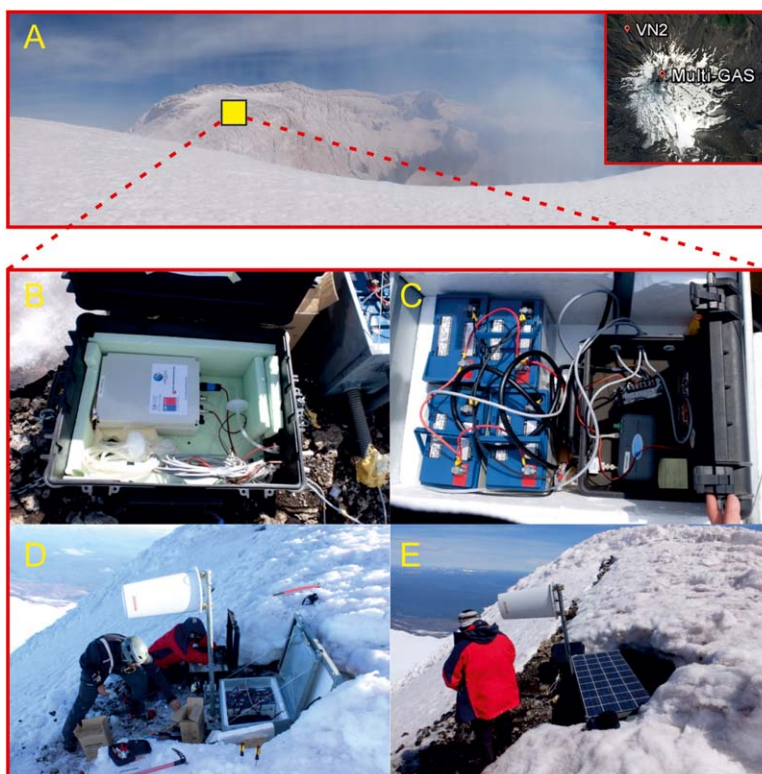


**Figure 2.** Images demonstrating the Multi-GAS deployment on 12 November 2014. (a) Location of the Multi-GAS site on the Villarrica summit (the inset is a Google Earth map of Villarrica volcano, also showing the location of the VN2 seismic station, which data are used in this study); (b) the Multi-GAS housed in a waterproof-case; (c) metal box housing 4 batteries and the waterproof-case shown in the previous image; (d and e) solar panel and antenna.

approximately 1 month of escalating bubble bursting activity at the crater starting in early February, associated with high levels of seismicity and infrasound ([GVP, 2016] based on reports by Observatorio Volcanológico de los Andes del Sur, OVDAS, Servicio Nacional de Geología y Minería). Due to a progressive increase in reduced displacement and amplitude of volcanic tremor, the Villarrica alert level was raised to yellow on 6 February. On 3 March, strombolian activity increased further in vigour and then transitioned at ~3:00 AM (local time) to lava fountain activity, with fountains reaching ~1500 m above vent altitudes [GVP, 2016]. This violent VEI 2 paroxysm lasted about half an hour, but produced intense tephra fallout, scoria flows and a 20 km long lahar [Johnson and Palma, 2015].

### 3. Material and Methods

A fully autonomous Multi-GAS was deployed on 12 November 2014 on the eastern outer rim of Villarrica crater, at an altitude of 2870 m a.s.l (coordinates: 39°25'15" S, 71°56'21" W) (Figure 2a). Deployment was conducted by UniPa-INGV-OVDAS personnel (M.B. V.F. and C.B) as part of the Volcanic Deep Earth Carbon Degassing (DECADE) project of the Deep Carbon Observatory ([https://deepcarbon.net/dco\\_project\\_summary?uri=http://info.deepcarbon.net/individual/n7907](https://deepcarbon.net/dco_project_summary?uri=http://info.deepcarbon.net/individual/n7907)). The Multi-GAS was housed in a small waterproof-case (Figure 2b), also containing a Moxa embedded computer (model 7112plus) that commanded the Multi-GAS operations. The waterproof-case was fit inside a metal box along-side with 4 batteries (Figure 2c), and the telemetry system (FGR2-PE 900 MHz Industrial Ethernet Radio; from FreeWave Technologies). The cover of the metal box was fit to a 120 W solar panel and an antenna (Figures 2d and 2e), pointed toward a radio master OVDAS station on the volcano's eastern slope. This telemetry system granted regular data streaming to OVDAS servers where data were stored.

The Villarrica Multi-GAS employed the same sensors as in previous work [e.g., Aiuppa *et al.*, 2014]. In particular, we used a Gascard EDI030102NG infra-red spectrometer from Edinburgh Instruments (accuracy,  $\pm 1.5\%$ ),



2 electrochemical sensors for SO<sub>2</sub> (T3ST/F - TD2G-1A) and H<sub>2</sub>S (T3H - TC4E-1A) both from City Technology (repeatability, 1%) and a KVM3/5 Galltec-Mela T/Rh sensor. The Multi-GAS operated from 13 November 2014 (0 AM local time) to 1 March 2015 (0.30 AM local time), when data flow to OVDAS servers ceased. A reconnaissance survey carried out on the crater days after the 3 March paroxysm confirmed the Multi-GAS had been buried underneath a thick cover of spatter deposited during the vigorous explosive activity of 1–3 March (Figure 1). In the 13 November to 1 March interval, the Multi-GAS worked continuously, excepted for a single data gap between 20 December and 11 January, due to heavy snowfall and consequent icing of the instrument's inlet (as verified in a reconnaissance survey in late-December). During operation, the Multi-GAS measured (at 0.1 Hz rate) the in-plume concentrations of CO<sub>2</sub>, SO<sub>2</sub> and H<sub>2</sub>S during 4 daily measurement cycles (0–0.30; 6–6.30; 12–12.30; 18–18.30; all Local Time). Ambient pressure, temperature and relative humidity were also measured, which allowed calculation of in-plume H<sub>2</sub>O concentrations using the Arden Buck equation [Buck, 1981]. The volcanic H<sub>2</sub>O signal (of a few thousands ppmv) was resolved from the overwhelming background (ambient) air H<sub>2</sub>O concentration (2500–10,000 ppmv) from analysis of co-acquired SO<sub>2</sub> concentrations (being only 20 ppb in ambient air). In particular, a polynomial function was fit to sets of H<sub>2</sub>O readings with contemporaneous SO<sub>2</sub>  $\sim 0$  [Aiuppa et al., 2010c]. The so-obtained background air H<sub>2</sub>O content was subtracted from H<sub>2</sub>O readings to obtain volcanic H<sub>2</sub>O. No H<sub>2</sub>S was detected above the 13% cross-sensitivity of the H<sub>2</sub>S sensor to SO<sub>2</sub> [Tamburello, 2015].

We postprocess the acquired CO<sub>2</sub> and SO<sub>2</sub> concentration data using the Ratiocalc software [Tamburello, 2015] to obtain time-averaged CO<sub>2</sub>/SO<sub>2</sub> ratios calculated over 30 min long Multi-GAS acquisition windows. The obtained results are listed in Table 1. Results are only reported for temporal windows in which the SO<sub>2</sub> concentration was above a 5 ppmv threshold, and in which high correlations ( $R^2 \geq 0.7$ ) between CO<sub>2</sub> and SO<sub>2</sub> concentrations were observed. Each temporal window included 50 to 200 measurements, and the size of the window was automatically adapted in Ratiocalc to maximize the correlation coefficient. Based on laboratory tests, we assess the overall errors at  $\leq 15\%$  and  $\leq 30\%$  for the derived CO<sub>2</sub>/SO<sub>2</sub> and H<sub>2</sub>O/CO<sub>2</sub> ratios.

#### 4. Results

The CO<sub>2</sub> and SO<sub>2</sub> concentrations measured by the Villarica summit crater Multi-GAS instrument are illustrated in the temporal plot of Figure 3b. The Multi-GAS almost continually detected SO<sub>2</sub> concentrations well above the background atmosphere level ( $\sim 20$  ppb), implying persistent volcanic gas plume fumigation at our measurement site (Figure 3b). CO<sub>2</sub> concentrations also typically exceeded the normal atmospheric levels ( $\sim 400$  ppmv), and fluctuated around a  $\sim 420$ – $470$  ppmv baseline (Figure 3b). Median concentrations of SO<sub>2</sub> and CO<sub>2</sub> of  $5.4 \pm 5$  and  $476 \pm 23$  ppmv, respectively, were observed between 13 November 2014 and 5 February 2015 and represent typical background degassing (Figure 3b). The median SO<sub>2</sub> and CO<sub>2</sub> concentrations then increased between 6 February and 1 March 2015 to  $9.2 \pm 14$  and  $488 \pm 54$  ppmv, indicating elevated degassing (Figure 3b). The peak SO<sub>2</sub> and CO<sub>2</sub> concentrations were also far larger after 6 February (respectively of 122 and 1043 ppmv) than in the 13 November 2014 to 5 February 2015 period (45 and 550 ppmv, respectively). Interestingly, gas concentrations increased simultaneously with an abrupt increase in seismicity (Real-time Seismic-Amplitude Measurement, RSAM; Figure 3a), that induced OVDAS to raise the volcano's alert level to yellow on 6 February.

The time-averaged CO<sub>2</sub>/SO<sub>2</sub> ratios, calculated in individual 30 min-long Multi-GAS acquisition windows, are illustrated in the temporal plot of Figure 3c. Based on the temporal record of volcanic gas CO<sub>2</sub>/SO<sub>2</sub> ratios, we identify three distinct phases. During *Background degassing Phase I* (13 November 2014 to 25 January 2015), the derived CO<sub>2</sub>/SO<sub>2</sub> ratios were systematically lower than 3 (range 0.65–2.7), and mostly comprised between 1 and 2 (all ratios reported here and below are on molar basis). Starting from January 26, in what we refer to as *Phase II* (26 January 26 to 5 February), the CO<sub>2</sub>/SO<sub>2</sub> ratios fluctuated more widely, and peak values as high as 8.3 were noticed. Both visual observations and measurements (e.g., stable pressure readings on the Multi-GAS) indicate that no closing/icing of the inlet or any other malfunctioning occurred, implying the CO<sub>2</sub>/SO<sub>2</sub> difference between *Phase I* and *II* is real, and not an instrumental drift effect. The mean CO<sub>2</sub>/SO<sub>2</sub> ratio for *Phase II* was 2.1 (Figure 4), or slightly higher than in *Phase I*. Fluctuating, high (up to 9.1) CO<sub>2</sub>/SO<sub>2</sub> ratios persisted also during the *Phase III* (same as in Figure 3b) that preceded the 3 March paroxysm. The mean CO<sub>2</sub>/SO<sub>2</sub> ratio for *Phase III* was 2.7, or the highest between the 3 periods.

**Table 1.** Multi-GAS Derived Volcanic Gas Plume Ratios From Villarrica Volcano<sup>a</sup>

Date	CO <sub>2</sub> /SO <sub>2</sub>	H <sub>2</sub> O/CO <sub>2</sub>	Date	CO <sub>2</sub> /SO <sub>2</sub>	H <sub>2</sub> O/CO <sub>2</sub>	Date	CO <sub>2</sub> /SO <sub>2</sub>	H <sub>2</sub> O/CO <sub>2</sub>
13/11/2014 00:04	1.2	19.5	31/01/2015 06:24	3.0	14.8	18/02/2015 18:09	4.3	5.4
14/11/2014 00:27	1.5	42.2	31/01/2015 12:06	1.9	10.9	19/02/2015 06:25	3.2	6.8
14/11/2014 06:14	2.1	7.5	31/01/2015 18:13	2.2	9.6	19/02/2015 12:06	2.5	6.2
14/11/2014 12:14	1.3	24.5	01/02/2015 00:04	3.4	11.6	19/02/2015 18:07	4.0	n.d.
15/11/2014 06:24	1.4	19.1	01/02/2015 06:22	2.4	10.3	20/02/2015 00:12	3.0	8.4
15/11/2014 18:26	1.2	79.4	01/02/2015 12:03	7.1	8.3	20/02/2015 06:04	3.7	n.d.
16/11/2014 00:18	0.8	35.5	01/02/2015 12:03	3.6	16.4	20/02/2015 12:13	3.1	n.d.
19/11/2014 12:10	1.2	n.d.	01/02/2015 12:26	2.6	23.2	20/02/2015 18:16	1.7	23.6
19/11/2014 18:28	0.6	n.d.	02/02/2015 00:12	2.0	29.2	21/02/2015 00:06	1.4	13.5
23/11/2014 00:18	2.1	n.d.	02/02/2015 06:25	3.3	n.d.	21/02/2015 06:14	1.9	22.0
23/11/2014 04:35	1.2	n.d.	02/02/2015 18:24	0.7	131.9	21/02/2015 12:09	2.5	14.6
23/11/2014 06:23	1.5	n.d.	02/02/2015 18:27	1.7	n.d.	21/02/2015 18:05	3.1	5.3
24/11/2014 12:25	1.2	n.d.	03/02/2015 18:06	2.1	n.d.	22/02/2015 12:16	2.1	9.1
24/11/2014 18:25	1.5	n.d.	04/02/2015 00:12	3.3	25.3	22/02/2015 18:17	1.9	13.0
25/11/2014 00:15	1.9	n.d.	04/02/2015 06:19	3.8	21.3	23/02/2015 00:15	1.5	12.9
25/11/2014 06:24	1.2	n.d.	04/02/2015 12:12	5.9	n.d.	23/02/2015 06:04	3.4	19.6
25/11/2014 12:26	0.7	8.7	04/02/2015 18:05	2.6	16.0	24/02/2015 00:00	1.9	11.5
26/11/2014 12:22	1.1	12.2	04/02/2015 18:25	2.4	n.d.	24/02/2015 06:15	1.6	12.8
27/11/2014 12:15	1.9	17.9	05/02/2015 06:13	3.7	12.4	24/02/2015 12:14	2.8	4.7
28/11/2014 18:10	1.7	11.2	05/02/2015 06:22	3.3	n.d.	25/02/2015 00:12	2.4	8.4
29/11/2014 18:11	1.2	28.2	05/02/2015 18:04	1.5	36.6	25/02/2015 06:12	2.8	6.0
30/11/2014 12:01	1.9	21.2	05/02/2015 18:07	2.3	n.d.	25/02/2015 12:11	3.1	n.d.
01/12/2014 06:09	1.1	9.0	05/02/2015 18:17	0.9	n.d.	25/02/2015 18:06	2.1	8.1
02/12/2014 00:26	0.9	18.8	06/02/2015 00:13	2.0	12.0	26/02/2015 00:06	1.7	15.1
03/12/2014 06:14	1.3	15.4	06/02/2015 00:19	2.4	n.d.	26/02/2015 06:00	2.7	5.2
03/12/2014 18:07	1.3	16.8	06/02/2015 06:05	2.3	38.6	26/02/2015 12:11	2.8	7.6
04/12/2014 00:11	1.4	14.3	06/02/2015 06:13	1.9	n.d.	26/02/2015 18:08	2.4	6.6
04/12/2014 06:21	1.2	19.6	06/02/2015 06:22	1.4	n.d.	27/02/2015 06:10	3.4	3.6
04/12/2014 18:07	1.2	48.3	06/02/2015 12:14	1.6	16.0	27/02/2015 12:16	2.9	12.3
05/12/2014 00:19	1.7	47.8	06/02/2015 12:23	1.4	n.d.	27/02/2015 18:14	3.8	n.d.
05/12/2014 18:05	2.0	17.9	06/02/2015 18:06	1.5	53.3	28/02/2015 00:09	2.2	14.4
06/12/2014 00:14	1.6	14.0	07/02/2015 00:12	1.9	16.9	28/02/2015 12:20	2.5	n.d.
06/12/2014 06:04	1.9	n.d.	07/02/2015 06:06	1.9	12.4	28/02/2015 18:24	1.3	32.5
08/12/2014 00:13	1.3	n.d.	07/02/2015 06:10	1.6	n.d.	01/03/2015 00:25	2.4	2.8
08/12/2014 12:16	1.3	16.9	07/02/2015 12:03	1.9	11.3			
08/12/2014 18:16	0.8	62.1	07/02/2015 12:11	3.1	n.d.			
09/12/2014 00:26	1.5	5.7	07/02/2015 12:24	5.0	n.d.			
10/12/2014 00:01	1.8	n.d.	07/02/2015 18:06	2.2	13.5			
10/12/2014 06:06	2.6	7.1	07/02/2015 18:16	2.9	n.d.			
10/12/2014 12:23	2.7	9.3	07/02/2015 18:27	2.3	n.d.			
11/12/2014 06:25	2.7	n.d.	08/02/2015 00:06	3.8	5.5			
12/12/2014 12:24	1.5	16.6	08/02/2015 00:18	3.2	n.d.			
12/12/2014 18:19	1.5	25.6	08/02/2015 06:05	4.3	4.2			
13/12/2014 00:14	1.5	17.1	08/02/2015 06:10	3.6	n.d.			
14/12/2014 18:15	1.6	28.4	08/02/2015 06:15	5.3	n.d.			
15/12/2014 00:16	2.2	n.d.	08/02/2015 12:08	3.4	6.7			
15/12/2014 06:27	2.3	n.d.	08/02/2015 12:17	3.6	n.d.			
16/12/2014 06:15	2.4	5.8	08/02/2015 12:25	3.3	n.d.			
16/12/2014 12:09	1.9	12.4	09/02/2015 00:06	3.6	19.5			
16/12/2014 18:03	2.1	17.9	09/02/2015 00:12	3.3	n.d.			
17/12/2014 06:16	1.7	10.0	09/02/2015 00:15	3.0	n.d.			
17/12/2014 06:22	1.5	n.d.	09/02/2015 00:23	5.3	n.d.			
18/12/2014 06:21	1.6	14.5	09/02/2015 00:23	4.3	n.d.			
14/01/2015 00:13	1.3	n.d.	09/02/2015 06:03	5.0	n.d.			
14/01/2015 06:27	1.8	n.d.	09/02/2015 06:08	6.7	n.d.			
14/01/2015 12:08	2.3	8.3	09/02/2015 06:25	5.3	n.d.			
14/01/2015 18:02	1.2	n.d.	09/02/2015 18:07	5.0	5.4			
15/01/2015 12:19	1.4	n.d.	10/02/2015 00:03	2.7	10.0			
15/01/2015 18:24	1.9	n.d.	10/02/2015 06:09	2.4	23.9			
17/01/2015 12:19	1.7	14.9	10/02/2015 12:05	3.2	7.5			
22/01/2015 18:18	1.1	29.6	10/02/2015 18:10	1.9	25.2			
23/01/2015 00:17	2.4	5.6	11/02/2015 00:10	2.0	5.5			
23/01/2015 06:16	1.7	20.6	11/02/2015 06:09	1.3	28.3			
23/01/2015 12:10	1.1	31.8	11/02/2015 12:15	1.8	6.6			
23/01/2015 18:03	1.7	22.6	11/02/2015 18:12	2.6	38.2			
24/01/2015 00:17	1.9	17.9	12/02/2015 00:23	1.2	32.7			
24/01/2015 06:10	2.0	18.7	12/02/2015 06:23	2.1	0.7			
25/01/2015 00:15	2.6	n.d.	12/02/2015 12:26	1.6	10.4			

Table 1. (continued)

Date	CO <sub>2</sub> /SO <sub>2</sub>	H <sub>2</sub> O/CO <sub>2</sub>	Date	CO <sub>2</sub> /SO <sub>2</sub>	H <sub>2</sub> O/CO <sub>2</sub>	Date	CO <sub>2</sub> /SO <sub>2</sub>	H <sub>2</sub> O/CO <sub>2</sub>
25/01/2015 06:16	1.4	n.d.	12/02/2015 18:14	1.2	24.5			
25/01/2015 12:10	2.0	n.d.	13/02/2015 00:20	1.0	15.0			
25/01/2015 18:21	1.8	n.d.	13/02/2015 06:03	1.4	22.5			
26/01/2015 00:05	3.7	9.6	13/02/2015 12:09	0.9	26.2			
26/01/2015 06:16	3.8	6.8	13/02/2015 18:24	1.8	n.d.			
26/01/2015 12:17	2.7	18.6	14/02/2015 12:12	2.3	n.d.			
26/01/2015 18:04	4.5	n.d.	15/02/2015 00:21	2.4	14.9			
27/01/2015 00:01	4.5	n.d.	15/02/2015 00:21	3.1	n.d.			
27/01/2015 06:11	3.4	11.7	15/02/2015 06:19	2.4	12.8			
27/01/2015 12:01	2.7	n.d.	15/02/2015 06:19	2.2	n.d.			
27/01/2015 18:09	1.8	19.5	15/02/2015 18:21	2.1	n.d.			
28/01/2015 00:23	3.0	n.d.	16/02/2015 00:11	2.0	11.9			
28/01/2015 06:23	0.9	28.1	16/02/2015 06:10	4.0	6.4			
28/01/2015 12:05	0.8	70.7	16/02/2015 12:10	3.6	8.4			
29/01/2015 00:18	8.3	n.d.	16/02/2015 18:09	2.6	13.5			
29/01/2015 12:17	5.6	12.6	17/02/2015 00:24	1.8	19.8			
29/01/2015 18:25	0.7	125.9	17/02/2015 12:10	1.3	31.7			
30/01/2015 00:08	4.8	11.2	17/02/2015 18:12	1.5	18.5			
30/01/2015 06:12	3.1	3.8	18/02/2015 00:07	5.0	6.9			
30/01/2015 12:22	2.6	12.9	18/02/2015 06:19	3.1	11.7			
31/01/2015 00:22	0.7	37.2	18/02/2015 12:06	9.1	1.4			

<sup>a</sup>All ratios are molar. Date are given in dd/mm/yyyy hh:minmin format (time identifies the central time of the acquisition window processed with Ratiocalc to derive the quoted ratio).

This time-changing degassing regime is also confirmed by the CO<sub>2</sub> vs. SO<sub>2</sub> scatter plot of Figure 4. The diagram demonstrates that *Phase I*, apart from being characterized by lower gas concentrations, was also associated with lower CO<sub>2</sub>/SO<sub>2</sub> ratios, as indicated by the slope of the best-fit regression line ( $R^2 = 0.5$ ) being  $\sim 1.8$ . In contrast, in the *Phase III* of 6 February to 1 March 2015, the CO<sub>2</sub> versus SO<sub>2</sub> dependence was less dispersed ( $R^2 = 0.7$ ) and steeper (slope of the best-fit regression line, 3.2). This confirms that, after 6 February, CO<sub>2</sub> degassing increased with respect to SO<sub>2</sub> degassing.

In some selected temporal windows (Table 1), a volcanic H<sub>2</sub>O signal of a few thousands ppmv, in excess to the background (ambient) air (2500–10,000 ppmv H<sub>2</sub>O), was resolved. This volcanic excess H<sub>2</sub>O was identified based on the positive, high ( $R_2 > 0.7$ ) correlations with both SO<sub>2</sub> and CO<sub>2</sub> concentrations. Based on these correlations (same methodology as in Aiuppa *et al.* [2014]), we inferred the volcanic gas H<sub>2</sub>O/CO<sub>2</sub> ratios listed in Table 1. The derived H<sub>2</sub>O/CO<sub>2</sub> ratios varied widely, from 1.3 to 132, and inversely correlated with CO<sub>2</sub>/SO<sub>2</sub> (Figure 5). The H<sub>2</sub>O/CO<sub>2</sub> compositions observed for *Phase I*, *II* and *III* subpopulations were somewhat overlapping (Figure 5). However, the derived compositions for *Phase III* were less hydrous (H<sub>2</sub>O/CO<sub>2</sub> ratios  $< 38$ ), and all data-points with CO<sub>2</sub>/SO<sub>2</sub>  $> 3$  were systematically associated with H<sub>2</sub>O/CO<sub>2</sub> ratios  $< 20$  (and mostly within 1.3 and 8.3; Figure 5 and Table 1).

## 5. Discussion

### 5.1. An Unusually CO<sub>2</sub>-Rich Gas for Villarrica

Our novel volcanic gas results here demonstrate a “perturbed” degassing regime for Villarrica in the weeks prior to the 3 March 2015 paroxysm (Figures 3 and 6). Our derived CO<sub>2</sub>/SO<sub>2</sub> ratios (0.65 to 2.7) for the *Phase I* are well within the range of previous gas reports (CO<sub>2</sub>/SO<sub>2</sub> ratios between 0.69 and 2.2; see Figure 6). These compositions are consistent with the relatively low CO<sub>2</sub>/SO<sub>2</sub> ratio composition of Villarrica gas during background activity [Shinohara and Witter, 2005], and with the relatively CO<sub>2</sub>-poor nature of magmas feeding the “normal” lava-lake activity at Villarrica [Witter *et al.*, 2004]. These low magmatic carbon contents in both glass inclusions ( $\leq 0.1$  wt. %) [Witter *et al.*, 2004] and volcanic gases [Shinohara and Witter, 2005] possibly suggest limited carbon transport from the slab into the mantle wedge magmatic source [Aiuppa *et al.*, 2015]. Since 26 January (onset of *Phase II*), however, the recorded gas composition became manifestly more CO<sub>2</sub>-rich, with peak CO<sub>2</sub>/SO<sub>2</sub> ratios up to  $\approx 9$ , or a factor 4–13 higher than during regular activity (Figure 6). This variation in gas composition preceded, by  $\approx 10$  days, the observed escalation in seismic activity since 6 February (Figure 3). This anomalous CO<sub>2</sub>-rich composition persisted, although with fluctuations, for several consecutive weeks (e.g., CO<sub>2</sub>/SO<sub>2</sub> ratio of  $\approx 9$  on 18 February). Our last observations (28 February to 1 March),

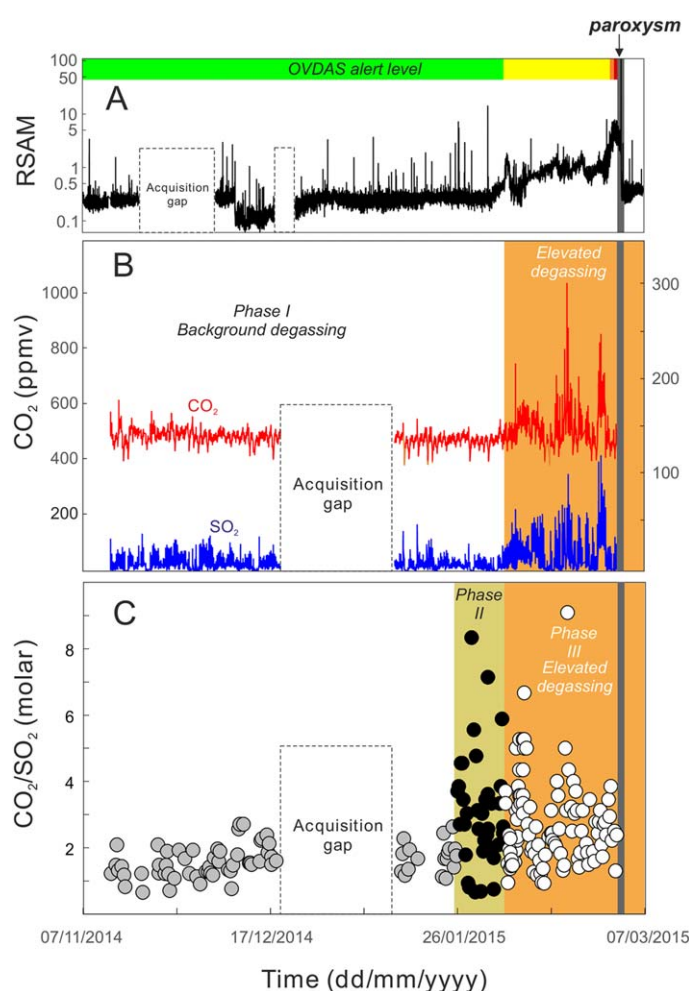


**Figure 3.** Temporal records of (a) Real-time Seismic-Amplitude Measurement (RSAM) [Endo and Murray, 1991] taken from the VN2 station, located ~4 km northeast of the Villarrica crater (see inset in Figure 2a). Seismic data were filtered in the 0.4–9 Hz range to maximize the signal/noise ratio. This 0.4–9 Hz frequency range includes the majority of seismic energy irradiated by Villarrica, and is poorly affected by nonvolcanic (meteorological) effects [Palma et al., 2008]. (b) CO<sub>2</sub> and SO<sub>2</sub> concentrations at the Villarrica Multi-GAS site and (c) derived CO<sub>2</sub>/SO<sub>2</sub> ratios. In Figure 3a, the sequence of alert levels issued by OVDAS is also indicated. Each point in Figure 3c represents the mean CO<sub>2</sub>/SO<sub>2</sub> ratio obtained from processing of CO<sub>2</sub> and SO<sub>2</sub> concentration data (using the Ratiocalc software [Tamburello, 2015]) acquired in an individual 30 min-long Multi-GAS acquisition window (data from Table 1). Three distinct degassing periods (Phases I, II, and III) are identified (see text).

used the estimated values of 2.1 and 0.1 wt. % from Shinohara and Witter [2005]. According to the authors, these volatile contents imply melt saturation at ~260 MPa pressure. Our simulations were performed in both closed-system (200–0.1 MPa range) and open-system conditions (Tab. 2). In the latter case, we assumed that the melt becomes open to gas loss from either 100 or 20 MPa pressure (open-system degassing was then maintained down to 0.1 MPa in both cases). Calculations on glass inclusions [Witter et al., 2004] indicated entrapment temperatures of ~1135°C and redox conditions between the nickel-nickel oxide (NNO) for olivine-hosted glass inclusions and up to 1 log-unit above NNO for plagioclase-hosted glass inclusions. This range of redox conditions was therefore explored in our simulations (Tab. 1).

Our model results are illustrated in Figures 7 and 8. Models predict a pressure-dependent evolution of the magmatic gas CO<sub>2</sub>/S<sub>T</sub> ratio that is qualitatively similar to that inferred for other volcanoes [Edmonds, 2008], see the Etna volcano example shown in Figure 7 for comparison (data from Aiuppa et al., [2007]). At any condition explored (open or closed, NNO or NNO+1), the model runs output a magmatic gas phase

taken right before communication with the summit Multi-GAS was lost during escalation of volcanic activity, suggested declining CO<sub>2</sub>/SO<sub>2</sub> ratios (1.3–2.5; see Tab. 1). In summary, our observations here are reminiscent of the cycles of CO<sub>2</sub>/SO<sub>2</sub> ratios increase/decrease seen prior to eruption of other volcanoes such as Etna [Aiuppa et al., 2007, 2010a; Patanè et al., 2013], Redoubt [Werner et al., 2013] or Turrialba [de Moor et al., 2016].

## 5.2. Constraints From Volatile Saturation Models

We attempt to quantitatively interpret our observations by comparing the measured volcanic gas compositions with model results obtained with the volatile saturation code of Moretti et al. [2003] and Moretti and Papale [2004] (Figures 7 and 8). As in previous work [Aiuppa et al., 2007], we used this saturation code to calculate the pressure-dependent evolution of the magmatic gas phase exsolved from Villarrica magmas upon their migration and decompression in the upper crust. Table 2 lists the input parameters for the model runs. The dry melt composition used in the simulations (Tab. 2) corresponds to the most volatile-rich melt inclusion of Witter et al. [2004], which contained 1.4 wt. % H<sub>2</sub>O, 920 ppm S and 530 ppm Cl. For the parental melt H<sub>2</sub>O and CO<sub>2</sub> contents, we

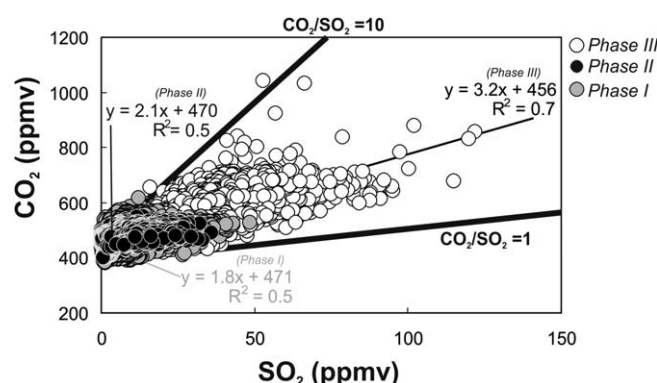


**Figure 4.** Scatter plot of  $\text{CO}_2$  vs.  $\text{SO}_2$  in-plume concentrations measured at the Villarrica Multi-GAS site. Measurements taken in the different phases (I–III) are plotted separately. Equations are best-fit regression lines (and correlation coefficients) for the three distinct periods. The slope of each regression line identifies the characteristic  $\text{CO}_2/\text{SO}_2$  ratio of each phase.

$S_T$  ratio is steeper, so that rapid  $\text{CO}_2$  loss from the melt leads to highly  $\text{CO}_2$ -depleted gas ( $\text{CO}_2/S_T$  ratio of  $\leq 0.1$  at  $\leq 15$  MPa pressure) that is not seen in the natural data set (Figures 3b and 5). In the open system assumption, the measured volcanic gas range (0.65–9.1) would therefore imply high (30–35 MPa) equilibration pressures, or at the upper range of the closed-system estimates above.

Reasonable agreement between modeled and measured (volcanic gas) compositions is also observed in the  $\text{H}_2\text{O}-\text{CO}_2-S_T$  magmatic gas system, see Figure 8. Closed-system model degassing trends actually plot at the  $\text{H}_2\text{O}$ -poor range of the volcanic gas data set (Figure 8). This might suggest either higher parental melt  $\text{H}_2\text{O}$  contents for Villarrica magmas than used in our model runs (2.1 wt. %), or more oxidized ( $> \text{NNO}+1$ ) redox conditions than recorded by glass inclusions. We cannot exclude, however, that part of the mismatch between modeled and measured gas compositions simply reflect the Multi-GAS over-estimating the real volcanic  $\text{H}_2\text{O}$  signal. Resolving atmospheric vs. volcanic  $\text{H}_2\text{O}$  signals in Multi-GAS temporal records is often complicated by large, erratic temporal variations in ambient (background) air  $\text{H}_2\text{O}$  levels [Aiuppa *et al.*, 2014].

### 5.3. Implications for the Trigger Mechanism of the 3 March Paroxysm

The longevity of active lava lakes is commonly explained as resulting from convective uni-direction [Witham *et al.*, 2006] or bi-directional [Francis *et al.*, 1993; Oppenheimer and Francis, 1998; Harris *et al.*, 1999, 2005;

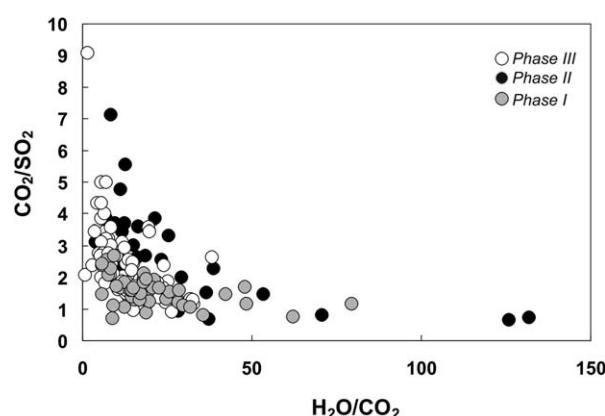


**Figure 5.** Scatter plot of  $\text{CO}_2/\text{SO}_2$  vs.  $\text{H}_2\text{O}/\text{CO}_2$  ratios in the Villarrica plume (data from Table 1). Data symbols as in Figure 4. The derived compositions for Phase III are generally characterized by lower ( $< 38$ )  $\text{H}_2\text{O}/\text{CO}_2$  ratios (with some overlap). High  $\text{CO}_2/\text{SO}_2$  ( $> 3$ ) ratios systematically correspond to low  $\text{H}_2\text{O}/\text{CO}_2$  ratios ( $< 20$ , but mostly in the 1.3–8.3 range).

(coexisting with Villarrica melt) that is  $\text{CO}_2$ -dominated at high pressure (Figure 7) ( $S_T$  here stands for total sulfur and is the combination of  $\text{SO}_{2(g)}$  and  $\text{H}_2\text{S}_{(g)}$ ). In the model runs, the  $\text{CO}_2/S_T$  ratio then decreases almost linearly upon pressure decrease and, in the closed-system runs, reaches low values ( $\text{CO}_2/S_T$  ratio of  $\sim 1$ ) at low (0.1–5 MPa) pressure. Comparison between such modeled (closed-system conditions) and natural (volcanic gas) data would therefore imply equilibration pressures for the gases we measured in 2014–2015 ( $\text{CO}_2/S_T$  ratios of 0.65–9.1) ranging from 0.1 to  $\sim 20$ –35 MPa (Figure 7). In open-system conditions, the pressure dependence of the  $\text{CO}_2/S_T$

ratio is steeper, so that rapid  $\text{CO}_2$  loss from the melt leads to highly  $\text{CO}_2$ -depleted gas ( $\text{CO}_2/S_T$  ratio of  $\leq 0.1$  at  $\leq 15$  MPa pressure) that is not seen in the natural data set (Figures 3b and 5). In the open system assumption, the measured volcanic gas range (0.65–9.1) would therefore imply high (30–35 MPa) equilibration pressures, or at the upper range of the closed-system estimates above.

Reasonable agreement between modeled and measured (volcanic gas) compositions is also observed in the  $\text{H}_2\text{O}-\text{CO}_2-S_T$  magmatic gas system, see Figure 8. Closed-system model degassing trends actually plot at the  $\text{H}_2\text{O}$ -poor range of the volcanic gas data set (Figure 8). This might suggest either higher parental melt  $\text{H}_2\text{O}$  contents for Villarrica magmas than used in our model runs (2.1 wt. %), or more oxidized ( $> \text{NNO}+1$ ) redox conditions than recorded by glass inclusions. We cannot exclude, however, that part of the mismatch between modeled and measured gas compositions simply reflect the Multi-GAS over-estimating the real volcanic  $\text{H}_2\text{O}$  signal. Resolving atmospheric vs. volcanic  $\text{H}_2\text{O}$  signals in Multi-GAS temporal records is often complicated by large, erratic temporal variations in ambient (background) air  $\text{H}_2\text{O}$  levels [Aiuppa *et al.*, 2014].

**5.3. Implications for the Trigger Mechanism of the 3 March Paroxysm**

The longevity of active lava lakes is commonly explained as resulting from convective uni-direction [Witham *et al.*, 2006] or bi-directional [Francis *et al.*, 1993; Oppenheimer and Francis, 1998; Harris *et al.*, 1999, 2005; Oppenheimer *et al.*, 2004, 2009; Huppert and Hallworth, 2007; Harris, 2008; Palma *et al.*, 2011; Burgi *et al.*, 2014; Molina *et al.*, 2015] magma flow within the lake feeding conduit. At Villarrica, a bi-directional flow model is invoked, in which up-flowing gas-rich buoyant magma coexists in the conduit with down-flowing dense, degassed magma [Palma *et al.*, 2008, 2011]. The lack of periodicities in gas and thermal records possibly implies that the two magma types efficiently mix in the conduit [Moussallam *et al.*, 2016].

In addition to vertical magma motion, the role of large, over-pressurized gas bubbles has increasingly been implicated as a driving force in recent models of lava lake dynamics [Witham *et al.*, 2006; Witham and Llewellyn, 2006; Stix, 2007; Bouche *et al.*, 2010; Vergnolle and Bouche, 2016]. According to



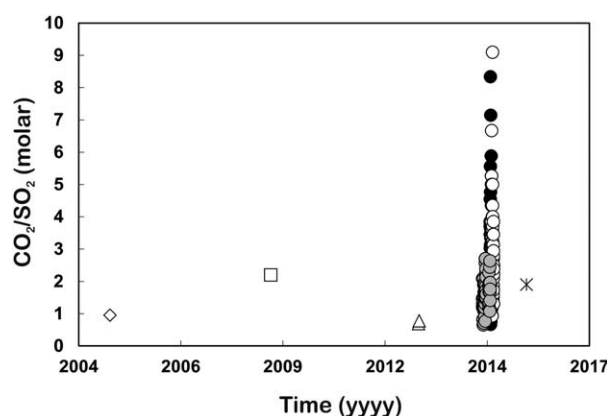


**Figure 6.** Temporal record of  $\text{CO}_2/\text{SO}_2$  ratios in the Villarrica plume. Data source: diamond [Shinohara and Witter, 2005]; Square [Sawyer et al., 2011]; triangles (This study, Multi-GAS observations taken between 25 February and 4 March 2013 by Y.M., N.P. and A.C); circles (this study, data from Table 1); star [Moussallam et al., 2016].

observed [Calder et al., 2004; Palma et al., 2008; Rose et al., 2013; Moussallam et al., 2016]. However, vigour and frequency of such bubble-bursting activity fluctuates over time [Richardson et al., 2014], and includes mild “seething magma” activity but also more energetic strombolian explosions and small lava fountains [Palma et al., 2008]. Calculations by Bouche et al. [2010] indicate that, at rheology and gas bubble volume conditions typical of Villarrica magmas [Gurioli et al., 2008], gas bubbles rising in the conduit may form bubbly wakes that, by repeated coalescence events, generate strombolian explosions or small lava fountaining events [Palma et al., 2008]. Seismic and infrasonic records [Richardson et al., 2014] are consistent with increases in bubble bursting activity being related to periodic injection of more gas bubble-rich magma in the conduit. When this happens, the level of the lava lake rises, strombolian explosions and lava

these models, the separate ascent of over-pressurized gas bubbles in the lake’s feeding conduit is the driver of active degassing (e.g., seething magma, strombolian explosions and lava fountains) at the lake surface [Palma et al., 2008], and would also act as to rejuvenate the lava lake itself by keeping it molten [Bouche et al., 2010]. It has also been proposed that a time-changing influx of gas bubbles from a “deeper” reservoir could be the cause for the lava level fluctuations recurrently seen at active lava lakes [Witham et al., 2006; Witham and Llewellyn, 2006; Stix, 2007; Vergnolle and Bouche, 2016], although not all observations are consistent with this idea [e.g., Peters et al., 2014].

At Villarrica, bursting of gas bubbles at the surface of the lava lake is continually observed [Calder et al., 2004; Palma et al., 2008; Rose et al., 2013; Moussallam et al., 2016]. However, vigour and frequency of such bubble-bursting activity fluctuates over time [Richardson et al., 2014], and includes mild “seething magma” activity but also more energetic strombolian explosions and small lava fountains [Palma et al., 2008]. Calculations by Bouche et al. [2010] indicate that, at rheology and gas bubble volume conditions typical of Villarrica magmas [Gurioli et al., 2008], gas bubbles rising in the conduit may form bubbly wakes that, by repeated coalescence events, generate strombolian explosions or small lava fountaining events [Palma et al., 2008]. Seismic and infrasonic records [Richardson et al., 2014] are consistent with increases in bubble bursting activity being related to periodic injection of more gas bubble-rich magma in the conduit. When this happens, the level of the lava lake rises, strombolian explosions and lava fountains become more frequent, and more energetic seismo-acoustic signals are detected [Richardson et al., 2014]. Clearly, the escalating seismic (Figure 3c) and explosive (Figure 1) activity that occurred in the month before the 3 March 2015 paroxysm sits at the upper limit of the spectrum of the activity pulses periodically interspersed within the regular Villarrica activity.

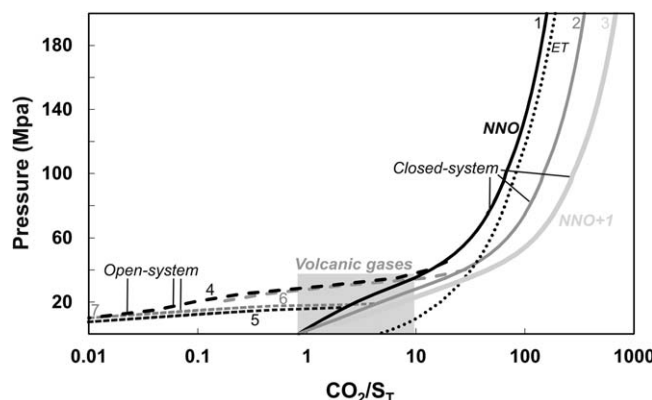


**Figure 7.** Model-predicted, pressure-dependent evolution of the  $\text{CO}_2/\text{S}_T$  ratio in the magmatic gas coexisting with a Villarrica-like melt (see Table 2 for model inputs).  $\text{S}_T$  stands for total sulfur, and was calculated by summing up  $\text{SO}_{2(g)}$  and  $\text{H}_2\text{S}_{(g)}$  concentrations returned by the model at each pressure step. Seven distinct model lines are shown. Models 1–3 were obtained by running closed-system simulations of magma depressurization (200–0.1 MPa range) over a range of redox conditions (from the nickel-nickel oxide buffer (NNO), to 1 log-unit above NNO (NNO+1)). Runs 4–7 were obtained by assuming open-system degassing conditions from either 100 or 20 MPa pressure (see Table 2). For comparison, the dotted curve labeled “ET” is a reference (closed-system) degassing trend for a Etna volcano, here taken as illustrative of a  $\text{CO}_2$ -rich magmatic system (the model curve is from Aiuppa et al. [2007], and refers to an hawaiite with initial  $\text{CO}_2$  and S contents of 2 and 0.3 wt. %). The yellow area identifies the inferred source pressures of volcanic gases released by Villarrica in 2014–2015, as based on their measured  $\text{CO}_2/\text{SO}_2$  ratios (these corresponds to  $\text{CO}_2/\text{S}_T$  since  $\text{H}_2\text{S}_{(g)}$  was below detection in the plume).

Our gas observations and models here suggest the role of deeply sourced bubbles in controlling the fluctuating Villarrica lava lake activity. The low (<3) volcanic gas  $\text{CO}_2/\text{S}_T$  compositions, seen in previous studies [Shinohara and Witter, 2005; Sawyer et al., 2011; Moussallam et al., 2016] and during our Phase I (Figures 3–6), agree well with model gas compositions obtained in closed-system conditions at pressures of 0.1–5 MPa. This match suggests that, during the regular Villarrica degassing activity, gas bubbles are not effectively separated from the melt until near-surface conditions are

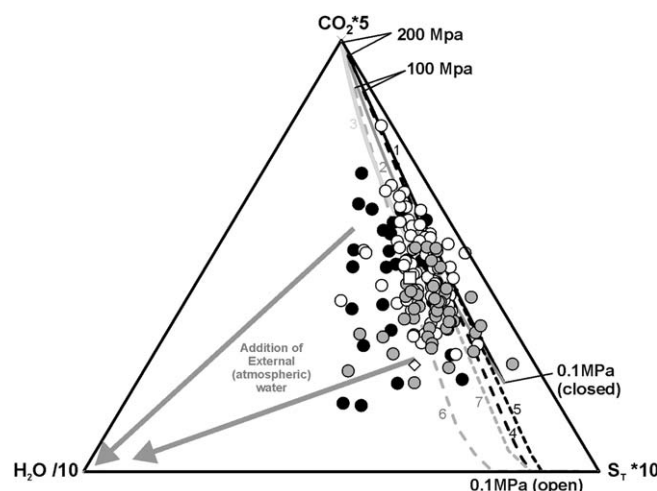


**Figure 8.** Triangular plot comparing model-predicted (lines as in Fig. 7) and observed (volcanic gases; Tab. 1) gas compositions in the  $H_2O/10$ - $CO_2 \cdot 5$ - $Sr \cdot 10$  magmatic system. Symbols of gas samples are as in Figures 2 and 6. A fair agreement between modeled and measured volcanic gas compositions is observed. Although the populations of gas samples taken during Phases I–III exhibit some level of overlap, samples of Phases II–III of Villarrica activity in 2015 are overall shifted toward more  $CO_2$ -enriched compositions, implying a “deeper” source origin for the feeding gas bubbles. The most  $H_2O$ -enriched gas samples (e.g., those that depart from the main data cluster and from the model lines) likely reflect some level of external (atmospheric)  $H_2O$ . For example, that subtraction during postprocessing of the background (ambient air) contribution to the Multi-GAS sensed  $H_2O$  was not entirely successful.

MPa (closed-system runs) to 30–35 MPa (open-system runs) (Figure 7), dominated the volcano’s surface emissions. We propose such “deep” signature of the Villarrica gas plume was evidence for a larger than normal supply of deeply sourced  $CO_2$ -rich gas bubbles. Interestingly, in Phase II, the volcanic gas  $CO_2/SO_2$  ratio increase was not paralleled by any sizeable increase in seismicity and bubble-bursting activity (Figure 3a), suggesting that  $CO_2$ -rich gas bubbles initially rose through (and vented from) the conduit quiescently (e.g., with no over-pressure development). We propose these  $CO_2$ -rich bubbles were initially sourced by deeply intruding, primitive (volatile-rich) magma. In Phase III, the gas composition became even more  $CO_2$ -rich (mean  $CO_2/SO_2$  ratio of 2.7 vs. 2.1 in Phase II), pointing to further increase in gas bubble transport in the upper conduit, this time paralleled by increasing seismicity (RSAM; Figure 3a). We argue that gas bubble accumulation/coalescence in the shallow magma feeding system, perhaps combined with further ascent

reached; or, in other words, that gas bubbles and melt remain coupled (in a closed-system environment) during most part of the magma convective circulation path that sustains the volcano’s open-vent activity [Witter *et al.*, 2004]. Since bubble bursting and mild explosive activity are persistently observed at Villarrica during regular activity [Calder *et al.*, 2004; Palma *et al.*, 2008], some extent of separate gas bubble flow in the conduit must in fact occur. We argue however that, during regular activity, active degassing contributes a minor fraction of the total Villarrica volatile budget, which we assume is dominated by passive (quiescent) volatile loss at the lake surface.

In contrast, the  $CO_2$ -rich volcanic gas compositions we observed since 26 January 2014 (Phases II and III) are not consistent with near-surface gas-melt equilibrium, but rather imply that deeply rising gas bubbles, originating at (minimum) pressures of  $\sim 20$ –35

**Table 2.** Input Parameters of Volatile Saturation Model Runs<sup>a</sup>

RUN ID	Temperature (°C) [Witter <i>et al.</i> , 2004]	Redox Conditions [Witter <i>et al.</i> , 2004]	Run Conditions (Pressure Range)	Melt Composition [Witter <i>et al.</i> , 2004; Shinohara and Witter, 2005]
1	1135	NNO	Closed from 200 to 0.1 MPa	$SiO_2 = 53.9$
2	“““	NNO+0.5	Closed from 200 to 0.1 MPa	$TiO_2 = 1.69$
3	“““	NNO+1	Closed from 200 to 0.1 MPa	$Al_2O_3 = 14.0$
4	“““	NNO	Closed from 200 to 100 MPa	$FeO_T = 11.4$
5	“““	NNO	Open from 100 to 0.1 MPa	$MnO = 0.22$
6	“““	NNO+1	Closed from 200 to 20 MPa	$MgO = 5.0$
7	“““	NNO+1	Open from 100 to 0.1 MPa	$CaO = 8.7$
				$Na_2O = 3.3$
				$K_2O = 0.99$
				$P_2O_5 = 0.38$
				$CO_2 = 0.106$
				$H_2O = 2.1$
				$S = 0.092$
				$Cl = 0.053$

<sup>a</sup>Run ID 1–7 identify model curves shown in Figures 7 and 8.

and degassing of the primitive magma batch, were the causal factors for the escalating explosive and seismic activity that culminated into the 3 March 2015 paroxysmal eruption. Shallow magma emplacement prior to the paroxysm is supported by declining  $\text{CO}_2/\text{SO}_2$  ratios (1.3–2.5) in 28 February to 1 March. Independent petrological information on geochemistry and texture of erupted volcanics are clearly required to confirm our  $\text{CO}_2$ -rich magma trigger for the paroxysm.

## 6. Conclusions

We have shown here that the Villarrica paroxysmal eruption of 3 March 2015 was preceded by circa 1 month of anomalously high  $\text{CO}_2/\text{SO}_2$  ratios in the volcanic gas plume. These results bring novel information on degassing dynamics of active lava lakes, and contribute preliminary models for the mechanisms that govern transition from regular activity to more explosive (paroxysmal) regimes. Comparison between volcanic gas observations and model simulations of volatile degassing suggests that the  $\text{CO}_2$ -rich gas vented by Villarrica prior to 3 March was sourced by at least 20–35 MPa pressure, which contrasts with a near-surface origin for the  $\text{CO}_2$ -poor gas measured during regular activity. We tentatively propose that unusual supply of deeply sourced gas bubbles to the shallow Villarrica feeding conduit, possibly sourced by deeply intruding primitive (volatile-rich) magma, was the trigger for the escalating explosive and seismic unrest in February to early March 2015. We additionally argue that the 3 March 2015 paroxysm was finally triggered by gas bubble accumulation/coalescence, perhaps combined with final shallow emplacement of the volatile-rich magma. Our results suggest a “deep” gas driver for fluctuations in lava lake activity at Villarrica, in contrast to other lava lakes (e.g., Halema’uma’u Crater, on Kilauea Volcano) for which a mechanism of shallow gas accumulation has been invoked [Patrick *et al.*, 2016].

## Acknowledgments

This work was funded by the DECADE research initiative of the DCO observatory. The authors wish to thank P. Kelly, T. Lopez and an anonymous reviewer for useful comments and suggestions upon reviewing the manuscript. Both raw (concentrations) and processed (ratios) data are downloadable from the EarthChem Library at <https://doi.org/10.1594/IEDA/100640>.

## References

- Aiuppa, A. (2015), Volcanic gas monitoring, in *Volcanism and Global Environmental Change*, edited by A. Schmidt, K. E. Fristad, and L. T. Elkins-Tanton, pp. 81–96, Cambridge Univ. Press, Cambridge, U. K.
- Aiuppa, A., C. Federico, G. Giudice, and S. Gurrieri (2005), Chemical mapping of a fumarolic field: La Fossa Crater, Vulcano Island (Aeolian Islands, Italy), *Geophys. Res. Lett.*, **32**, L13309, doi:10.1029/2005GL023207.
- Aiuppa, A., R. Moretti, C. Federico, G. Giudice, S. Gurrieri, M. Liuzzo, P. Papale, H. Shinohara, and M. Valenza (2007), Forecasting Etna eruptions by real-time observation of volcanic gas composition, *Geology*, **35**(12), 1115–1118.
- Aiuppa, A., et al. (2009), The 2007 eruption of Stromboli volcano: Insights from real-time measurement of the volcanic gas plume  $\text{CO}_2/\text{SO}_2$  ratio, *J. Volcanol. Geotherm. Res.*, **182** (3–4), 221–230, doi:10.1016/j.jvolgeores.2008.09.013.
- Aiuppa, A., et al. (2010a), Patterns in the recent 2007–2008 activity of Mount Etna volcano investigated by integrated geophysical and geochemical observations, *Geochem. Geophys. Geosyst.*, **11**, Q09008, doi:10.1029/2010GC003168.
- Aiuppa, A., et al. (2010b), Unusually large magmatic  $\text{CO}_2$  gas emissions prior to a basaltic paroxysm, *Geophys. Res. Lett.*, **37**, L17303, doi:10.1029/2010GL043837.
- Aiuppa, A., et al. (2010c), A model of degassing for Stromboli volcano, *Earth Planet. Sci. Lett.*, **295**, 195–204.
- Aiuppa, A., P. Robidoux, G. Tamburello, V. Conde, B. Galle, G. Avar, E. Bagnato, J. M. De Moor, M. Martínez, and A. Muñoz (2014), Gas measurements from the Costa Rica-Nicaragua volcanic segment suggest possible along-arc variations in volcanic gas chemistry, *Earth Planet. Sci. Lett.*, **407**, 134–147.
- Aiuppa, A., P. Robidoux, and T. B. Fischer (2015), Along-arc and inter-arc variations in volcanic gas  $\text{CO}_2/\text{S}$  signature, *Geophys. Res. Abstr.*, **17**EGU2015-3773, Abstract presented at EGU General Assembly 2015.
- Aiuppa, A., T. B. Fischer, T. Plank, P. Robidoux and R. Di Napoli (2017), Along-arc, inter-arc and arc-to-arc variations in volcanic gas  $\text{CO}_2/\text{S}_\text{T}$  ratios reveal dual source of carbon in arc volcanism, *Earth Sci. Rev.*, **168**, 24–47.
- Allard, P., et al. (2015), Prodigious emission rates and magma degassing budget of major, trace and radioactive volatile species from Ambrym basaltic volcano, Vanuatu island Arc, *J. Volcanol. Geotherm. Res.*, **304**, 378–402.
- Allard, P., M. Burton, G. Sawyer, and P. Bani (2016), Degassing dynamics of basaltic lava lake at a top-ranking volatile emitter: Ambrym volcano, Vanuatu arc, *Earth Planet. Sci. Lett.*, **448**, 69–80.
- Bouche, E., S. Vergnolle, T. Staudacher, A. Nercessian, J.-C. Delmont, M. Frogneux, F. Cartault, and A. Le Pichon (2010), The role of large bubbles detected from acoustic measurements on the dynamics of Erta ‘Ale lava lake (Ethiopia), *Earth Planet. Sci. Lett.*, **295**(1–2), 37–48.
- Buck, A. L. (1981), New equations for computing vapor pressure and enhancement factor, *J. Appl. Meteorol.*, **20**, 1527–1532.
- Burgi, P.-Y., T. H. Darrah, D. Tedesco, and W. K. Eymold (2014), Dynamics of the Mount Nyiragongo lava lake, *J. Geophys. Res. Solid Earth*, **119**, 4106–4122, doi:10.1002/2013JB010895.
- Calder, E. S., A. J. L. Harris, P. Peña, E. Pilger, L. P. Flynn, H. Fuentealba, and H. Moreno (2004), Combined thermal and seismic analysis of the Villarrica Volcano lava lake, Chile, *Rev. Geol. Chile*, **31**(2), 259–272.
- de Moor, J. M., et al. (2016), Turmoil at Turrialba Volcano (Costa Rica): Degassing and eruptive processes inferred from high-frequency gas monitoring, *J. Geophys. Res., Solid Earth*, **121**, 5761–5775, doi:10.1002/2016JB013150.
- Edmonds, M. (2008), New geochemical insights into volcanic degassing, *Philos. Trans. R. Soc. A*, **366**(1885), 4559–4579.
- Endo, E. T., and T. Murray (1991), Real-time Seismic Amplitude Measurement (RSAM): A volcano monitoring and prediction tool, *Bull. Volcanol.*, **53**, 533–545, doi:10.1007/BF00298154.
- Fischer, T. P., and G. Chiodini (2015), Volcanic, magmatic and hydrothermal gas discharges, in *Encyclopaedia of Volcanoes*, 2nd ed., pp. 779–797, edited by H. Sigurdsson, et al., Academic Press, Amsterdam, doi:10.1016/B978-0-12-385938-9.00045-6.
- Francis, P., C. Oppenheimer, D. Stevenson (1993), Endogenous growth of persistently active volcanoes, *Nature*, **366**(6455), 554–557.

- Global Volcanism Program (GVP) (2013), Villarrica (357120), in *Volcanoes of the World*, v. 4.5.2., edited by E. Venzke, Smithsonian Inst., National Museum of Natural History, Washington, D. C., doi:10.5479/si.GVP.VOTW4-2013. [Available at <http://volcano.si.edu/volcano.cfm?vn=357120>.]
- Global Volcanism Program (GVP) (2016), Report on Villarrica (Chile), in *Bulletin of the Global Volcanism Network*, vol. 41:11, edited by E. Venzke, Smithsonian Inst., National Museum of Natural History, Washington, D. C. [Available at <https://volcano.si.edu/showreport.cfm?doi=10.5479/si.GVP.BGVN201611-357120>.]
- Goto, A., and J. B. Johnson (2011), Monotonic infrasound and Helmholtz resonance at Volcan Villarrica (Chile), *Geophys. Res. Lett.*, **38**, L06301, doi:10.1029/2011GL046858.
- Gurioli, L., A. J. L. Harris, B. F. Houghton, M. Polacci, and M. Ripepe (2008), Textural and geophysical characterization of explosive basaltic activity at Villarrica volcano, *J. Geophys. Res.*, **113**, B08206, doi:10.1029/2007JB005328.
- Harris, A. J. L. (2008), Modelling lava heat loss, rheology and convection, *Geophys. Res. Lett.*, **35**, L07303, doi:10.1029/2008GL033190.
- Harris, A. J. L., L. P. Flynn, D. A. Rothery, C. Oppenheimer, and S. B. Sherman (1999), Mass flux measurements at active lava lakes: Implication for magma recycling, *J. Geophys. Res.*, **104**(B4), 7117–7136.
- Harris, A. J. L., R. Carniel, and J. Jones (2005), Identification of variable convective regime at Erta 'Ale Lava Lake, *J. Volcanol. Geotherm. Res.*, **142**, 207–223.
- Hildreth, W., and S. Moorbath (1988), Crustal contributions to arc magmatism in the Andes, *Contrib. Mineral. Petrol.*, **98**, 455–489.
- Huppert, H., and M. Hallworth (2007), Bi-directional flows in constrained systems, *J. Fluid Mech.*, **578**, 95–112.
- Jacques, G., K. Hoernle, J. Gill, F. Hauff, H. Wehrmann, D. Garbe-Schönberg, P. van den Bogaard, I. Bindeman, and L. E. Lara (2013), Across-arc geochemical variations in the Southern Volcanic Zone, Chile (34.5–38.0°S): Constraints on mantle wedge and slab input compositions, *Chem. Geol.*, **371**(27–45), doi:10.1016/j.gca.2013.05.016.
- Johnson, J. B., and J. L. Palma (2015), Lahar infrasound associated with Volcán Villarrica's 3 March 2015 eruption, *Geophys. Res. Lett.*, **42**, 6324–6331, doi:10.1002/2015GL065024.
- Kamenetsky, V. S., M. Pompilio, N. Métrich, A. V. Sobolev, D. V. Kuzmin, and R. Thomas (2007), Arrival of extremely volatile-rich high-Mg magmas changes explosivity of Mount Etna, *Geology*, **35**(3), 255–258.
- Lopez, T., S. Ushakov, P. Izbekov, F. Tassi, C. Cahill, O. Neill, and C. Werner (2013), Constraints on magma processes, subsurface conditions, and total volatile flux at Bezymianny Volcano in 2007–2010 from direct and remote volcanic gas measurements, *J. Volcanol. Geotherm. Res.*, **263**, 92–107.
- Martin, R. S., et al. (2010), A total volatile inventory for Masaya Volcano, Nicaragua, *J. Geophys. Res.*, **115**, B09215, doi:10.1029/2010JB007480.
- Mather, T. A., V. I. Tsanev, D. M. Pyle, A. J. S. McGonigle, C. Oppenheimer, and A. G. Allen (2004), Characterization and evolution of tropospheric plumes from Láscar and Villarrica volcanoes, Chile, *J. Geophys. Res.*, **109**, D21303, doi:10.1029/2004JD004934.
- Métrich, N., P. Allard, N. Spilliaert, D. Andronico, and M. Burton (2004), 2001 flank eruption of the alkali- and volatile-rich primitive basalt responsible for Mount Etna's evolution in the last three decades, *Earth Planet. Sci. Lett.*, **228**(1–2), 1–17.
- Molina, I., A. Burgisser, and C. Oppenheimer (2015), A model of the geochemical and physical fluctuations of the lava lake at Erebus volcano, Antarctica, *J. Volcanol. Geotherm. Res.*, **308**, 142–157.
- Moreno, H., J. Clavero, and L. Lara (1994), Explosive post-glacial activity of Villarrica volcano, southern Andes, paper presented at 7<sup>th</sup> Congreso Geológico Chileno, Univ. of Concepcion, Concepcion, Chile.
- Moretti, R., and P. Papale (2004), On the oxidation state and volatile behaviour in multicomponent gas–melt equilibria, *Chem. Geol.*, **213**, 265–280, doi:10.1016/j.chemgeo.2004.08.048.
- Moretti, R., P. Papale, and G. Ottonello (2003), A model for the saturation of C–O–H–S fluids in silicate melts, in *Volcanic degassing*, *Geol. Soc. London Spec. Publ.*, **213**, 81–101.
- Moussallam, Y., C. Oppenheimer, B. Scaillet, F. Gaillard, P. Kyle, N. Peters, M. Hartley, K. Berlo, and A. Donovan (2014), Tracking the changing oxidation state of Erebus magmas, from mantle to surface, driven by magma ascent and degassing, *Earth Planet. Sci. Lett.*, **393**, 200–209.
- Moussallam, Y., C. Oppenheimer, B. Scaillet, I. Buisman, C. Kimball, N. Dunbar, A. Burgisser, I. C. Schipper, J. Andújar, and P. Kyle (2015), Megacrystals track magma convection between reservoir and surface, *Earth Planet. Sci. Lett.*, **413**, 1–12, doi:10.1016/j.epsl.2014.12.022.
- Moussallam, Y., et al. (2016), Sustaining persistent lava lakes: Observations from high-resolution gas measurements at Villarrica volcano, Chile, *Earth Planet. Sci. Lett.*, **454**, 237–247.
- Oppenheimer, C., and P. Francis (1998), Implications of longeval lava lake for geomorphological and plutonic processes at Erta 'Ale volcano, *J. Volcanol. Geotherm. Res.*, **80**, 101–111.
- Oppenheimer, C., A. J. S. McGonigle, P. Allard, M. J. Wooster, and V. Tsanev (2004), Sulfur, heat, and magma budget of Erta 'Ale lava lake, Ethiopia, *Geology*, **32**, 509–512.
- Oppenheimer, C., A. S. Lomakina, P. R. Kyle, N. G. Kingsbury, and M. Boichu (2009), Pulsatory magma supply to a phonolite lava lake, *Earth Planet. Sci. Lett.*, **284**(3–4), 392–398.
- Oppenheimer, C., R. Moretti, P. R. Kyle, A. Eschenbacher, J. B. Lowenstern, R. L. Hervig, and N. W. Dunbar (2011), Mantle to surface degassing of alkalic magmas at Erebus volcano, Antarctica, *Earth Planet. Sci. Lett.*, **306**(3–4), 261–271.
- Oppenheimer, C., T. P. Fischer, and B. Scaillet (2014), Volcanic degassing: Process and impact, in *Treatise on Geochemistry, The Crust*, 2nd ed. 4, edited by H. D. Holland and K. K. Turekian, pp. 111–179, Elsevier, Amsterdam.
- Palma, J. L., E. S. Calder, D. Basualto, S. Blake, and D. A. Rothery (2008), Correlations between SO<sub>2</sub> flux, seismicity, and outgassing activity at the open vent of Villarrica Volcano, Chile, *J. Geophys. Res.*, **113**, B10201, doi:10.1029/2008JB005577.
- Palma, J. L., S. Blake, and E. S. Calder (2011), Constraints on the rates of degassing and convection in basaltic open-vent volcanoes, *Geochim. Geophys. Geosyst.*, **12**, Q11006, doi:10.1029/2011GC003715.
- Patanè, D., et al. (2013), Insights into magma and fluid transfer at Mount Etna by a multiparametric approach: A model of the events leading to the 2011 eruptive cycle, *J. Geophys. Res. Solid Earth*, **118**, 3519–3539, doi:10.1002/jgrb.50248.
- Patrick, M. R., T. Orr, A. J. Sutton, E. Lev, and D. Fee (2016), Shallowly driven fluctuations in lava lake outgassing, Kilauea Volcano, Hawai'i, *Earth Planet. Sci. Lett.*, **433**, 326–338.
- Peters, N., C. Oppenheimer, P. Kyle, and N. Kingsbury (2014), Decadal persistence of cycles in lava lake motion at Erebus volcano, Antarctica, *Earth Planet. Sci. Lett.*, **395**, 1–12, doi:10.1016/j.epsl.2014.03.032.
- Plank, T. (2014), The chemical composition of subducting sediments, in *Treatise on Geochemistry, The Crust*, vol. 4, 2nd ed., edited by H. D. Holland and K. K. Turekian, pp. 607–629, Elsevier, Amsterdam.
- Richardson, J. P., G. P. Waite, and J. L. Palma (2014), Varying seismic-acoustic properties of the fluctuating lava lake at Villarrica volcano, Chile, *J. Geophys. Res. Solid Earth*, **119**, 5560–5573, doi:10.1002/2014JB011002.
- Ripepe, M., E. Marchetti, C. Bonadonna, A. J. L. Harris, L. Pioli, and G. Olivieri (2010), Monochromatic infrasonic tremor driven by persistent degassing and convection at Villarrica Volcano, Chile, *Geophys. Res. Lett.*, **37**, L15303, doi:10.1029/2010GL043516.



- Rose, W. I., J. L. Palma, H. Delgado Granados, and N. Varley (2013), Open-vent volcanism and related hazards: Overview, in *Understanding Open-Vent Volcanism and Related Hazard*, edited by W. I. Rose et al., *Geol. Soc. Am. Spec. Pap.*, 498, vii–xiii, doi:10.1130/2013.2498(00).
- Sadofsky, S. J., M. V. Portnyagin, K. Hoernle, and P. van den Bogaard (2008), Subduction cycling of volatile and trace elements through the Central American volcanic arc: Evidence from melt inclusions, *Contrib. Mineral. Petrol.*, 155(4), 433–456, doi:10.1007/s00410-007-0251-3.
- Sawyer, G. M., S. A. Carn, V. I. Tsanev, C. Oppenheimer, and M. R. Burton (2008a), Investigation into magma degassing at Nyiragongo volcano, democratic Republic of the Congo, *Geochem. Geophys. Geosyst.*, 9, Q02017, doi:10.1029/2007GC001829.
- Sawyer, G. M., C. Oppenheimer, V. I. Tsanev, and G. Yirgu (2008b), Magmatic degassing at Erta 'Ale volcano, Ethiopia, *J. Volcanol. Geotherm. Res.*, 178(4), 837–846.
- Sawyer, G. M., G. G. Salerno, J. S. Le Blond, R. S. Martin, L. Spampinato, T. J. Roberts, T. A. Mather, M. L. I. Witt, V. I. Tsanev, and C. Oppenheimer (2011), Gas and aerosol emissions from Villarrica volcano, Chile, *J. Volcanol. Geotherm. Res.*, 203, 62–75.
- Shinohara, H. (2005), A new technique to estimate volcanic gas composition: Plume measurements with a portable multi-sensor system, *J. Volcanol. Geotherm. Res.*, 143, 319–333.
- Shinohara, H., and J. B. Witter (2005), Volcanic gases emitted during mild Strombolian activity of Villarrica volcano, Chile, *Geophys. Res. Lett.*, 32, L20308, doi:10.1029/2005GL024131.
- Stern, C. R. (2004), Active Andean volcanism: Its geologic and tectonic setting, *Rev. Geol. Chile*, 31(2), 161–206.
- Stix, J. (2007), Stability and instability of quiescently active volcanoes: The case of Masaya, Nicaragua, *Geology*, 35, 535–538.
- Tamburello, G. (2015), Ratiocalc: Software for processing data from multicomponent volcanic gas analyzers, *Comput. Geosci.*, 82, 63–67.
- Tamburello, G., et al. (2015), Intense magmatic degassing through the lake of Copahue volcano, 2013–2014, *J. Geophys. Res. Solid Earth*, 120, 6071–6084, doi:10.1002/2015JB012160.
- Tamburello, G., T. H. Hansteen, S. Bredemeyer, A. Aiuppa, and F. Tassi (2014), Gas emissions from five volcanoes in northern Chile and implications for the volatiles budget of the Central Volcanic Zone, *Geophys. Res. Lett.*, 41, 4961–4969, doi:10.1002/2014GL060653.
- Van Daele M. et al. (2014), The 600 yr eruptive history of Villarrica Volcano (Chile) revealed by annually laminated lake sediments, *GSA Bull.*, 126(3/4), 481–498, doi:10.1130/B30798.1.
- Vergnolle, S., and E. Bouche (2016), Gas-driven lava lake fluctuations at Erta 'Ale volcano (Ethiopia) revealed by MODIS measurements, *Bull. Volcanol.*, 78, 60, 1–28.
- Wehrmann, H., K. Hoernle, G. Jacques, D. Garbe-Schönberg, K. Schumann, J. Mahlke, and L. E. Lara (2014), Volatile (sulphur and chlorine), major, and trace element geochemistry of mafic to intermediate tephra from the Chilean Southern Volcanic Zone (33–43°S), *Int. J. Earth Sci.*, 103(7), 1945–1962, doi:10.1007/s00531-014-1006-9.
- Werner, C., P. J. Kelly, M. Doukas, T. Lopez, M. Pfeffer, R. McGimsey, and C. Neal (2013), Degassing of CO<sub>2</sub>, SO<sub>2</sub>, and H<sub>2</sub>S associated with the 2009 eruption of Redoubt Volcano, Alaska, *J. Volcanol. Geotherm. Res.*, 259, 270–284.
- Witham, F., and W. Llewellyn (2006), Stability of lava lakes, *J. Volcanol. Geotherm. Res.*, 158, 321–332.
- Witham, F., A. W. Woods, and C. Gladstone (2006), An analogue experimental model of depth fluctuations in lava lakes, *Bull. Volcanol.*, 69(1), 51–56, doi:10.1007/s00445-006-0055-8.
- Witter, J. B., C. Victor, P. Kress, J. Delmelle, and J. Stix (2004), Volatile degassing, petrology, and magma dynamics of the Villarrica Lava Lake, Southern Chile, *J. Volcanol. Geotherm. Res.*, 134, 303–337.